Electronic Supplementary Material (ESI) for ChemComm.

Supporting Information

Coordination-driven assembly of a supramolecular square and oxidation to a tetra-ligand radical species

Khrystyna Herasymchuk,[a] Jessica J. Miller,[a] Gregory A. MacNeil,[a] Ania S. Sergeenko,[a] Declan McKearney,[a] Sébastien Goeb,[b] Marc Sallé,[b] Daniel B. Leznoff[a] and Tim Storr*[a]

[a] Department of Chemistry, Simon Fraser University, Burnaby, Canada.
E-mail: *tim_storr@sfu.ca

[b] Laboratoire MOLTECH-Anjou, UMR CNRS 6200, UNIV Angers, SFR MATRIX,
2 Bd Lavoisier, 49045 Angers Cedex, France

Table of Contents

1.0 Materials and Methods

All chemicals used were of the highest grade available and were further purified whenever necessary. $Pd(en)(NO_3)_2$ was synthesized according to a previous report.[1] The syntheses of the aldehyde precursors, 5-bromo-3-(*tert*-butyl)-2-hydroxybenzaldehyde (**1-Ald^{Br}**)[2] and 3-(*tert*-butyl)-2-hydroxy-5-(pyridin-4-yl)benzaldehyde (**2-Ald^{pPy}**)[3] and (R,R)-(–)-1,2-cyclohexanediamino-N,N'-bis(3-tert-butyl-5-(4-pyridyl)salicylidene) (**H_2Sal^{pPy}**)[4] have been previously reported. The tris(2,4-dibromophenyl)aminium hexafluoroantimonate radical chemical oxidant, $[N(C_6H_3Br_2)_3]^{\bullet+}[SbF_6]^-$ ($E_{1/2}$ = 1.14 V, MeCN)[5] was synthesized according to published protocols.[6] Electronic spectra were obtained on a Cary 5000 spectrophotometer with a custom-designed immersion fiber-optic probe with a path-length of 10 mm (Hellma, Inc.). Cyclic voltammetry (CV) was performed using a PAR-263A potentiometer, equipped with an Ag wire pseudo-reference electrode, a glassy carbon working electrode and a Pt counter electrode with $^nBu_4NPF_6$ (0.1 M) solutions in CH_3NO_2 under an inert atmosphere. Decamethylferrocene was used as an internal standard.[7] ^1H, ^{13}C and ^{31}P NMR spectra were recorded on a Bruker AV-400 or Bruker AVANCE II 600 MHz instruments and DOSY NMR was performed on Bruker AVANCE II 600 MHz instrument. Mass spectra were obtained on an Agilent 6210 (for **1**) and an IonSpec (Agilent), 9.4 T hybride ESI q-Q-q in CH_3NO_2 (10^{-3} M) (for **2**). Elemental analyses (C, H, N) were performed by Mr. Paul Mulyk at Simon Fraser University on a Carlo Erba EA 1110 CHN elemental analyzer. Infrared (IR) measurements were collected on a Thermo Nicolet Nexus 670 FT-IR spectrometer equipped with a Pike MIRacle attenuated total reflection (ATR) sampling accessory. All EPR spectra were collected using a Bruker EMXplus spectrometer operating with a premiumX X-band (~9.5 GHz) microwave bridge. Low temperature measurements (100 K and 253 K) of frozen solutions used a Bruker nitrogen temperature-control system and a continuous flow cryostat. Samples for X-band measurements were placed in 4 mm outer-diameter sample tubes with sample volumes of ~200 μL. Samples were prepared in capillaries with EPR tubes filled with toluene as an insulator for measurement at 253 K. STEM experiments were run on a FEI Tecnai Osiris S/TEM.

2.0 Synthesis

2.1 Synthesis of 1

A solution of $Ni(OAc)_2 \cdot 4H_2O$ (0.25 g, 1.0 mmol) in MeOH (20 mL) was added to a solution of H_2Sal^{pPy} (0.59 g, 1.0 mmol) in MeOH (20 mL), followed by triethylamine (0.28 mL, 2.0 mmol). The solution was then refluxed for 4 hours. Upon cooling of the reaction mixture, an olive-green precipitate was collected *via* vacuum filtration. The precipitate was washed with cold methanol. Crystals suitable for X-ray crystallography analysis were isolated via slow evaporation of a CH_2Cl_2 solution. Yield: (0.566 g, 88%). Elemental analysis (%) calcd for **1** ($C_{38}H_{42}N_4NiO_2$): C, 70.71; H, 6.56; N, 8.68. Found: C, 70.41; H, 6.70; N, 8.78. ESI-MS *m/z:* 645.27 ($[M+H]^+$, 100%). IR (ATR): 1591.95 cm^{-1} (s, ν_{as} (C=N) and ν_{as} (C=C)), 816.71 cm^{-1} (s, *w* (CH)). ^1H NMR (400 MHz, $CDCl_3$) δ 8.57 (s, 4H), 7.65-7.35 (m, 10H), 3.10 (br s, 2H), 2.56-2.46 (br m, 2H), 2.02-1.92 (br m, 2H), 1.47 (s, 18H), 1.40-1.31 (m, 4H). ^{13}C NMR (100 MHz, $CDCl_3$) δ 165.36, 158.16, 149.96, 141.90, 129.76, 129.01, 123.31, 120.87, 120.28, 70.08, 35.85, 29.55, 29.25, 28.88, 24.38.

2.2 Synthesis of 2

A solution of **1** (14 mg, 21.7 μmol) in THF (2.5 mL) was added to a solution of $Pd(en)(NO_3)_2$ (6.3 mg, 21.7 μmol) in H_2O (7.5 mL). NH_4PF_6 (70.7 mg, 0.434 mmol) was added to the orange solution after 2 hours of stirring at room temperature. The resultant mixture was further stirred at room temperature overnight. A red precipitate was then collected *via* vacuum filtration to afford **2**. Note **2** is used as the designation for $[\mathbf{2}]^{8+}(PF_6)_8$ in the manuscript. Yield: (22.8 mg, 96%). Elemental analysis (%) calcd for **2** ($C_{160}H_{200}F_{48}N_{24}Ni_4O_8P_8Pd_4$): C, 43.60; H, 4.57; N, 7.63. Found: C, 43.60; H, 4.58; N, 7.24. ESI-MS *m/z:* 736.6 ($[M-5PF_6^-]^{5+}$), 957.2 ($[M-4PF_6^-]^{4+}$), 1323.9 ($[M-3PF_6^-]^{3+}$). IR (ATR): 1592.91 cm^{-1} (w br, ν_{as} (C=N) and ν_{as} (C=C)), 840.81-837.92 cm^{-1} (s br, ν_{as} (FP) from PF_6). ^1H NMR (600 MHz, CD_3NO_2) δ 8.60 (t, J = 6.9 Hz, 4H), 7.82-7.60 (m, 10H), 4.26 (br s, 2H), 3.25-3.05 (m, 6H), 2.62-2.47 (m, 2H), 1.97-1.85 (m, 2H), 1.55-1.30 (m, 20H). ^{31}P NMR (162 MHz, CD_3NO_2) δ -144.56 (hept, J = 708.2 Hz, PF_6).

3.0 X-Ray Analysis

Single crystal X-ray crystallographic analysis of A was performed on a Bruker SMART ApexII Duo CCD diffractometer with a TRIUMPH graphite-monochromated Cu Kα (λ = 1.54184 Å) Incoatec microsource. Sample A was mounted on a MiTeGen dual-thickness MicroMounts using Paratone oil. Data was collected at 299 K in a series of φ and ω scans with 1.00˚ image widths and 15 and 30 second exposures. Additional crystallographic information can be found in Tables S1 in the Supporting Information and in cif format at CCDC deposition #1903336.

All single-crystal diffraction data were processed and initial solutions found with the Bruker ApexII software suite. Subsequent refinements were performed in SHELXL.[1] Hydrogen atoms for the molecule excluding the cyclohexyl backbone were added geometrically and refined using a riding model. The cyclohexyl ring was modeled as disordered, with hydrogens placed using the difference map and refined without constraint.

Table S1. Selected Crystallographic Data for **1**.

	1
Formula	$C_{38}H_{42}N_4NiO_2$
Formula weight	645.47
Crystal dimensions (mm)	0.050, 0.193, 0.267
Crystal system	Triclinic
Space group	P-1
a (Å)	11.0566(3)
b (Å)	12.9924(3)
*c (*Å)	13.9528(3)
α (°)	102.6010(10)
β (°)	107.7680(10)
γ (°)	112.9790(10)
V [Å^3]	1622.02(7)
Z	2
T (K)	299(2)
ρ_{calcd} (g cm^{-3})	1.322
μ (cm^{-1})	1.172
$2\theta_{max}$ (deg.)	66.707
Total reflections	5556
Observed reflections [$I_0 \geq 2\sigma(I_0)$]	5107
wR_2	0.1966
R_1	0.0740
GOF	1.250
Largest difference peak/hole (e-/ Å3)	0.726/-0.400

4.0 Scanning Transmission Electron Microscopy (STEM)

The 400 mesh Copper grid with Ultrathin Lacey Carbon film support was suspended onto a droplet of the solution containing **2** (100 μM) in CH_3CN. The grid was then placed onto a filter paper to absorb the excess of the remaining solution. Images were taken on a STEM 1 – FEI Tecnai Osiris operating at 200 kV and 225,000× magnification. The average particle diameter was measured using ImageJ software. At least 40 measurements were obtained per image (**Figure S3a**). Elemental mapping experiment on **2** (**Figure S3b**) confirmed the presence of both Ni (red) and Pd (green) in the sample, further supporting a self-assembly composition.

5.0 Calculation of the Diffusion Rate for 2 using the Randles-Sevcik Equation

The diffusion coefficient for **2** was estimated from cyclic voltammetry measurements at different scan rates:

$$i_{pa} = 2.69 \times 10^5 n^{\frac{3}{2}} A C_0 D_0^{\frac{1}{2}} v^{\frac{1}{2}} \quad (1)$$

where $\boldsymbol{i_{pa}}$ – anodic peak current (in amperes), $\boldsymbol{n}$ – number of electrons passed per molecule oxidized, $\boldsymbol{A}$ – area of the electrode (in cm^2), $\boldsymbol{C_0}$ – bulk concentration of the analyte (in moles/cm^3), $\boldsymbol{D_0}$ – diffusion coefficient of the analyte (in cm^2/s), $\boldsymbol{v}$ – potential scan rate (in V/s).

Plotting the change in current at the anode as a function of the square root of scan rate, provided a linear regression:

$$j_{pa} = f(v^{\frac{1}{2}}) \quad (2)$$

where

$$j_{pa} = \frac{i_{pa}}{A} \quad (3)$$

From the slope of the linear regression, D was calculated to be **2.22 × 10^{-10} m^2/s** for $n = 4$.

$$slope = 2.69 \times 10^5 n^{\frac{3}{2}} C_0 D_0^{\frac{1}{2}} \quad (4)$$

From the ^{1}H DOSY experiment, D was determined to be **2.45 × 10^{-10} m^2/s**.

The ratio of the experimentally determined D_{NMR} and D_{CV} for **2** is 1.10, which agrees with published approximation (Eq. 5) that accounts for different solvent system used in the NMR experiment (deuterated solvent) vs. electrochemistry experiment (solvent with supporting electrolyte).[8]

$$1.04 \times D_{NMR} = D_{CV} \quad (5)$$

6.0 Hydrodynamic Radius Calculation using the Stokes-Einstein Equation

The hydrodynamic radius, R_h, of **2** can be approximated using Stokes-Einstein equation (Eq. 6)[9] to be 1.48×10^{-9} m or 14.8 Å. The diffusion rate ($D = 2.45 \times 10^{-10}$ m^2/s) determined through ^{1}H DOSY experiment in CD_3NO_2 at 298 K was used for the calculation.

$$R_h = \frac{kT}{6\pi\eta D} \quad (6)$$

where $\boldsymbol{R_h}$ – hydrodynamic radius (in m), $\boldsymbol{k}$ – Boltzman constant (in J K^{-1}), $\boldsymbol{T}$ – temperature (in K), $\boldsymbol{\eta}$ – viscosity of the solvent (in Pa s), $\boldsymbol{D}$ – diffusion rate of the analyte (in m^2/s).

However, the calculated hydrodynamic radius (R_h = 14.8 Å) is likely inaccurate due to the non-spherical structure of **2**.[10] Hence the value does not correlate with the MMFF calculated size of **2**. Furthermore, the large pore size of **2**, likely contributes to a calculated hydrodynamic radius that is smaller than expected based on the MMFF calculation.[11]

7.0 UV-Vis-NIR Spectroscopy: Oxidation Protocol and Titration

Samples of $\mathbf{1}^+$ (0.25 mM) and $[\mathbf{2}]^{4\bullet+}$ (0.125 mM) in CH_3NO_2 were prepared at 253 K under nitrogen atmosphere in the immersion fiber-optic probe through the addition of a saturated solution of $[N(C_6H_3Br_2)_3]^{\bullet+}[SbF_6]^-$ in CH_2Cl_2 in 20 μL additions.

8.0 Electron Paramagnetic Resonance (EPR) Spectroscopy: Sample Preparation

Samples for EPR spectroscopy were prepared by taking an aliquot out of the immersion fiber-optic probe after 1 and 4 equivalents of $[N(C_6H_3Br_2)_3]^{\bullet+}[SbF_6]^-$ were added to CH_3NO_2 solutions

of **1** and **2**, respectively, under inert atmosphere and transferred into each EPR tube. EPR tubes containing the [**1**]$^{+}$ and [**2**]$^{4\bullet+}$ solutions were frozen at 77 K and stored until measurement at 100 K. Samples of **[2]**$^{4\bullet+}$ and $[N(C_6H_3Br_2)_3]^{\bullet+}[SbF_6]^{-}$ for EPR measurements at 253 K were prepared by placing each sample into a capillary, which was placed directly into an empty EPR tube.

9.0 Calculations

9.1 DFT and TD-DFT Calculations

Geometry optimization calculations for the [**fragment**]$^{+}$ (a 5^{+} cation) were completed using the Gaussian 16 program (Revision B.01),[12] the B3LYP[13] functional, the 6-31G(d) basis set (C, H, N, O, Ni), LanL2DZ[14] (Pd), with a polarized continuum model (PCM) for CH_2Cl_2 (dielectric ε = 8.94).[15] Frequency calculations at the same level of theory confirmed that the optimized structure was located at a minimum on the potential energy surface. Single-point calculations and the intensities of 10 lowest energy transitions using TD-DFT[16] calculations were performed using the B3LYP functional, the TZVP[17] basis set (C, H, N, O, Ni), LanL2DZ (Pd), with a PCM for CH_2Cl_2.

9.2 Molecular Mechanics Force Field (MMFF) Calculations

Merck Molecular Force Field (MMFF)[18] calculations were performed on **2** using *Spartan'18 Parallel Suite* from Wavefunction Inc. to obtain a potential ground state geometry and approximate size of the positively charged macrocycle (**Figure S2**). Counterions were omitted in the calculation. Calculations at a higher level of theory were not successful due to the size and charge of **2**. The diameter of **2** was also estimated *via* Stokes-Einstein equation utilizing DOSY NMR data, to be 29.6 Å (*vide supra*, **Section 6**).

10.0 Schemes and Figures

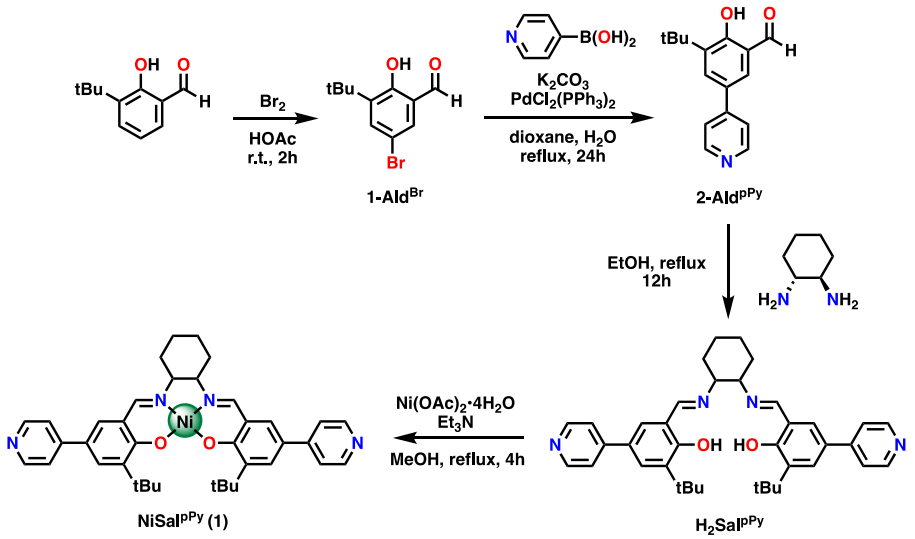

Scheme S1. Synthetic pathway to **1**

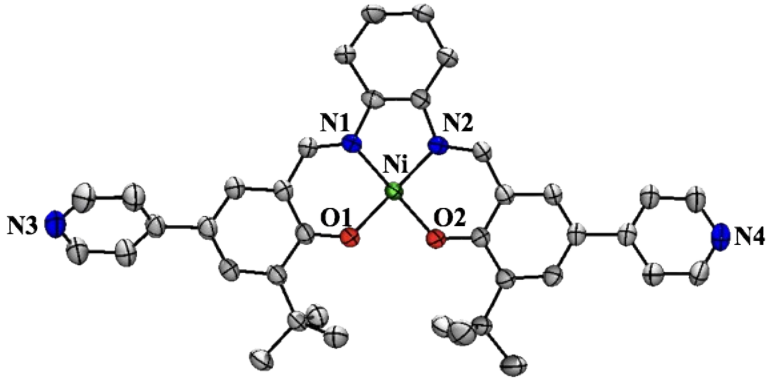

Figure S1. Crystal structure of **1**, hydrogen atoms excluded. Coordination sphere distances [Å] and angles [deg]: Ni-O(1): 1.842(4), Ni-O(2): 1.848(2), Ni-N(1): 1.845(3), Ni-N(2): 1.847(5); angles: O(1)-Ni-O(2): 85.2(1), O(1)-Ni-N(1): 94.3(2), O(1)-Ni-N(2): 177.6(2), O(2)-Ni-N(1): 178.1(2), O(2)-Ni-N(2): 94.5(2), N(1)-Ni-N(2): 86.0(2).

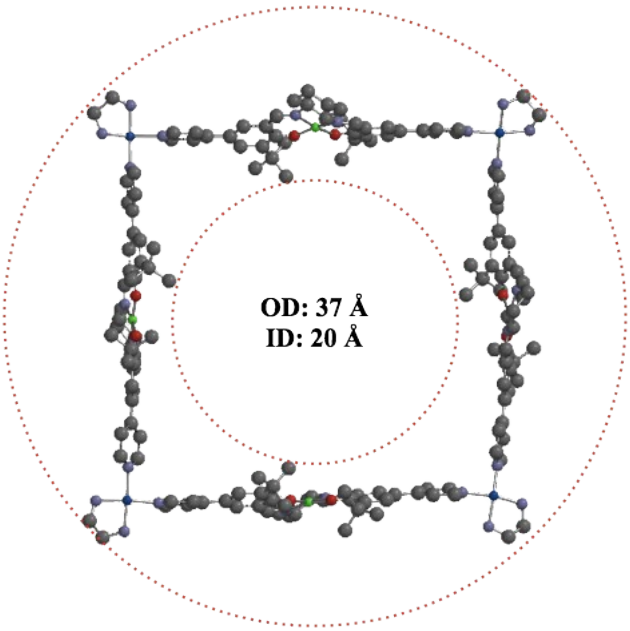

Figure S2. MMFF calculation of **2** (Outer diameter = 37 Å, Inner diameter = 20 Å).

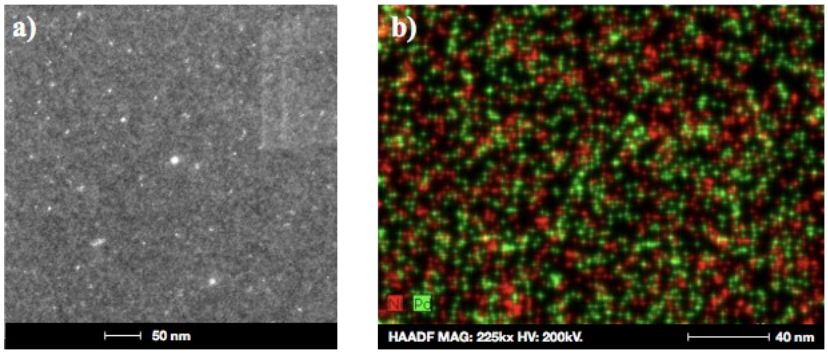

Figure S3. a) STEM image of **2**. b) STEM-Energy-dispersive X-ray (EDX) spectrum image of of Ni (red) and Pd (green), Conditions: 100 μM, magnification: 225,000 × .

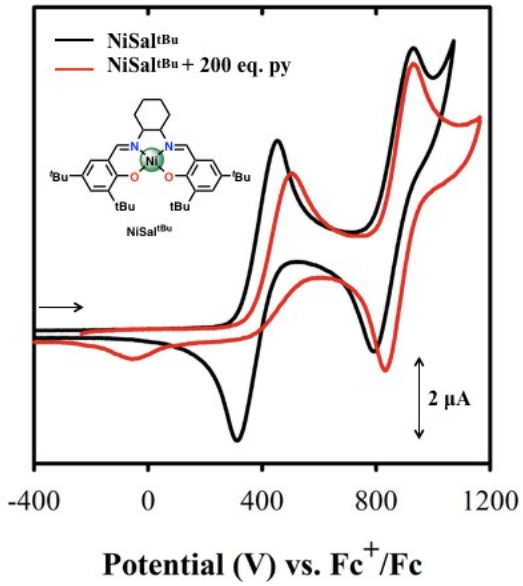

Figure S4. Cyclic voltammetry of **NiSal^{tBu}** (black) and **NiSal^{tBu} + 200 eq. of pyridine** (red). This experiment shows the change to an irreversible process for the first redox process in the presence of pyridine, due to axial pyridine binding to Ni. Conditions: 1.0 mM, with 0.1 M NBu_4ClO_4 in CH_2Cl_2 at 233 K.

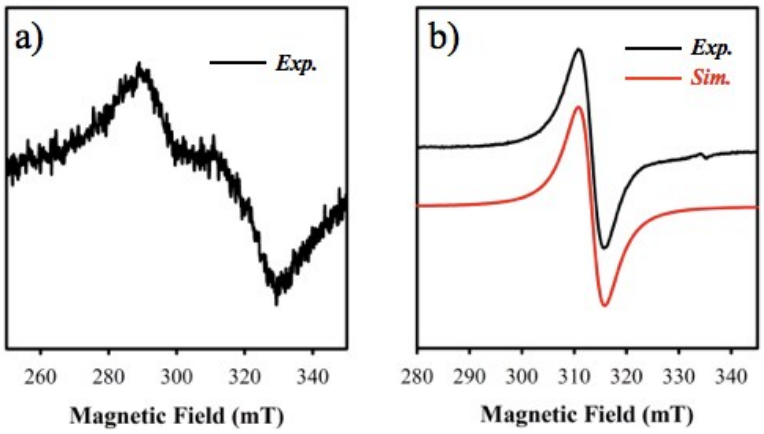

Figure S5. a) EPR of $[\mathbf{1}]^+$ (0.25 mM) in CH_3NO_2 at 100 K (estimated g_{avg} = 2.19); Low temperature measurements in CH_3NO_2 resulted in a broadened low intensity spectrum likely due to aggregation. b) EPR of $[\mathbf{1}]^+$ (0.5 mM) in CH_2Cl_2 at 100 K (g = 2.141); The oxidation of **1** in CH_2Cl_2 also results in the formation of Ni(III) species and an isotropic signal likely associated with aggregation upon intermolecular coordination of *para*-pyridyl groups. Conditions: frequency = 9.39 GHz, power = 2.0 mW, modulation frequency = 100 kHz, modulation amplitude = 0.6 mT.

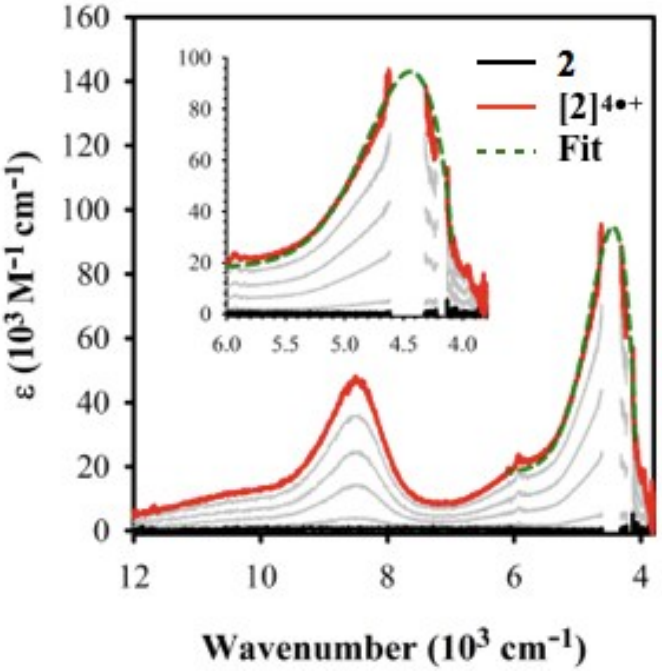

Figure S6. Electronic spectra of the chemical oxidation of **2** (0.125 mM, black) to $[\mathbf{2}]^{4\bullet+}$ (red), Gaussian fit of low energy NIR band (green); Solvent peaks were removed for clarity (between 4130-4220 cm^{-1} and 4320-4615 cm^{-1}). Conditions: in CH_3NO_2, at 253 K, titrated with 8 mM $[N(C_6H_3Br_2)_3]^{\bullet+}[SbF_6]^-$ as oxidant.

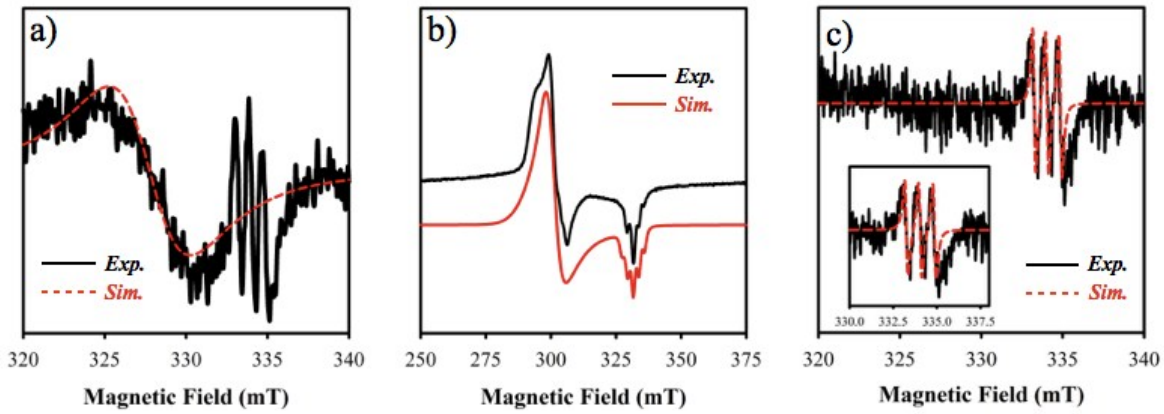

Figure S7. a) EPR of $[\mathbf{2}]^{4\bullet+}$ (0.5 mM) in CH_3NO_2 at 253 K (g_{avg} = 2.046). The spectrum confirms ligand radical formation upon oxidation of **2**. The low intensity of the signal is due to measurement in a capillary (polar solvent) combined with slow decay of $[\mathbf{2}]^{4\bullet+}$ in solution. An additional signal (three-line pattern), observed in the spectrum, matches the free oxidant $[N(C_6H_3Br_2)_3]^{\bullet+}[SbF_6]^-$ present in solution at g_{avg} = 2.008. b) EPR of $[\mathbf{2}]^{4+}$ (0.125 mM) in CH_3NO_2 at 100 K (g_1 =2.258, g_2 = 2.234, g_3 = 2.024, g_{avg} = 2.172, A_3 = 61 MHz); Low temperature measurements resulted in a rhombic S = ½ Ni(III)-phenolate complex. This spectrum of $[\mathbf{2}]^{4+}$ (characterized as Ni(III)) does not match that of $[\mathbf{1}]^{+}$ in **Figure S5a** (or **Figure S5b**), which is consistent with no disassembly of the macrocycle upon freezing. c) EPR of $[N(C_6H_3Br_2)_3]^{\bullet+}[SbF_6]^-$ (0.5 mM) in CH_3NO_2 at 253 K (g_{avg} = 2.008, A_3 = 23 MHz). Conditions for a) and c): frequency = 9.39 GHz, power = 2.0 mW, modulation frequency = 100 kHz, modulation amplitude = 1.0 mT. Conditions for b): frequency = 9.39 GHz, power = 2.0 mW, modulation frequency = 100 kHz, modulation amplitude = 0.6 mT.

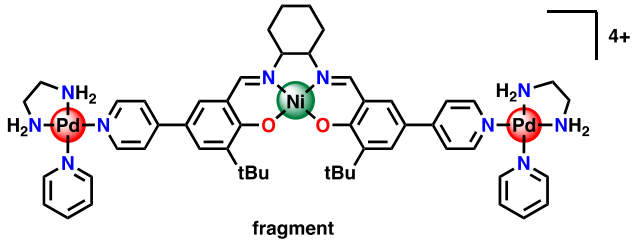

Figure S8. Structure of the **fragment** employed for DFT and TD-DFT calculations.

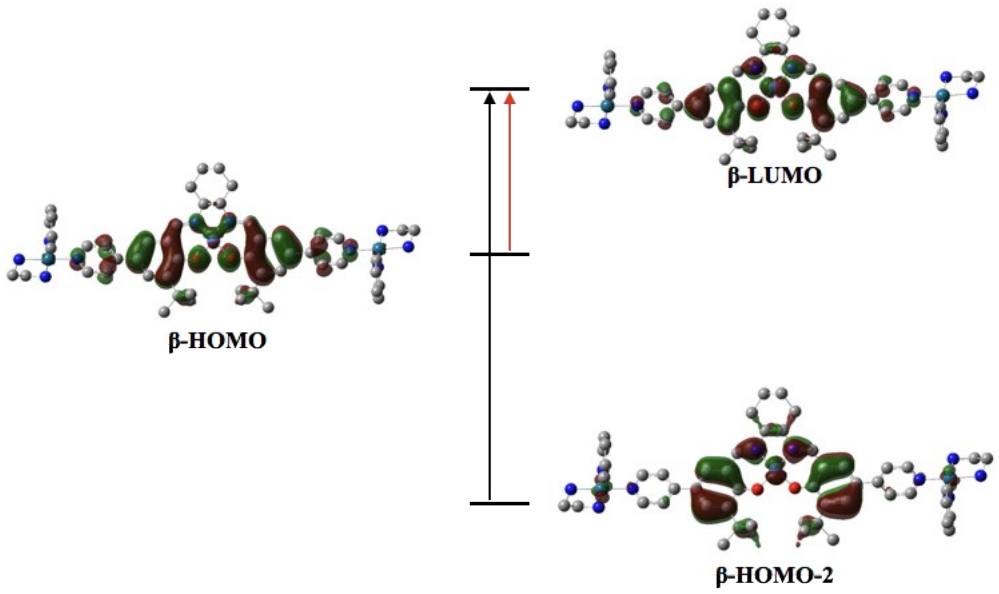

Figure S9. TD-DFT predicted low energy transitions for [**fragment**]$^{\bullet+}$. Calculated NIR transitions at 5240 cm^{-1} (red arrow; β-HOMO → β-LUMO (major contribution); oscillator strength, f = 0.2318) and 9650 cm^{-1} (black arrow; β-HOMO-2 → β-LUMO (major contribution); oscillator strength, f = 0.1247).

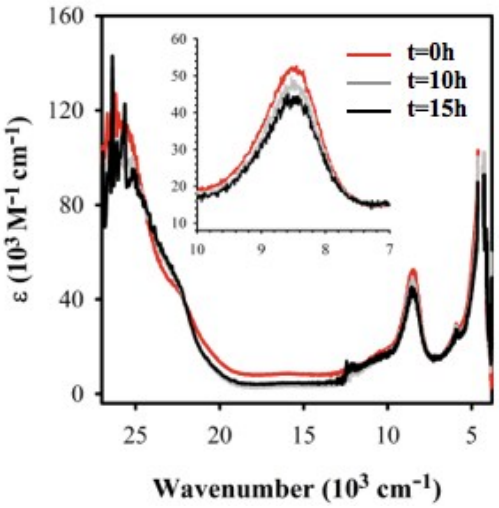

Figure S10. Electronic spectra of the decay of [**2**]$^{4\bullet+}$ (at t = 0 hr, 10 hr and 15 hr). Conditions: in CH_3NO_2, at 253 K, titrated with 8 mM $[N(C_6H_3Br_2)_3]^{\bullet+}[SbF_6]^-$ as oxidant.

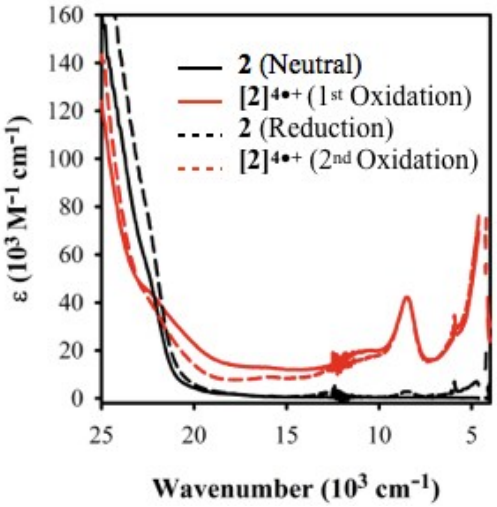

Figure S11. Electronic spectra of the regeneration of $[\mathbf{2}]^{4\bullet+}$: chemical oxidation of **2** (0.125 mM, black solid line) to $[\mathbf{2}]^{4\bullet+}$ (red solid line), chemical reduction of $[\mathbf{2}]^{4\bullet+}$ back to **2** (black dash line), second chemical oxidation of **2** to $[\mathbf{2}]^{4\bullet+}$ (red dash line). Conditions: in CH_3NO_2, at 253 K, titrated with 12 mM $[N(C_6H_3Br_2)_3]^{\bullet+}[SbF_6]^-$ as an oxidant and 18 mM $Fe(C_5(CH_3)_5)_2$ as a reductant.

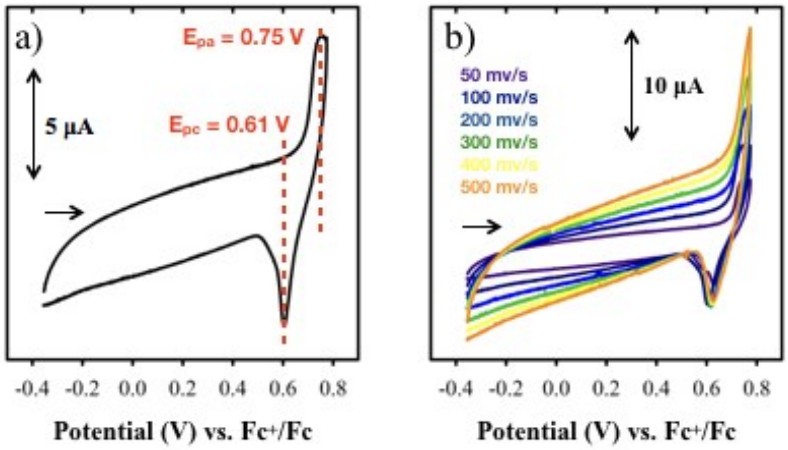

Figure S12. Cyclic voltammetry of **1** (0.50 mM, 100 mV/s) – scan direction reversed after reaching first redox process; b) Potential scan rate dependence of **1** (0.50 mM) 50-500 mV/s; Conditions: 0.1 M NBu_4PF_6 in CH_3NO_2 at 295 K.

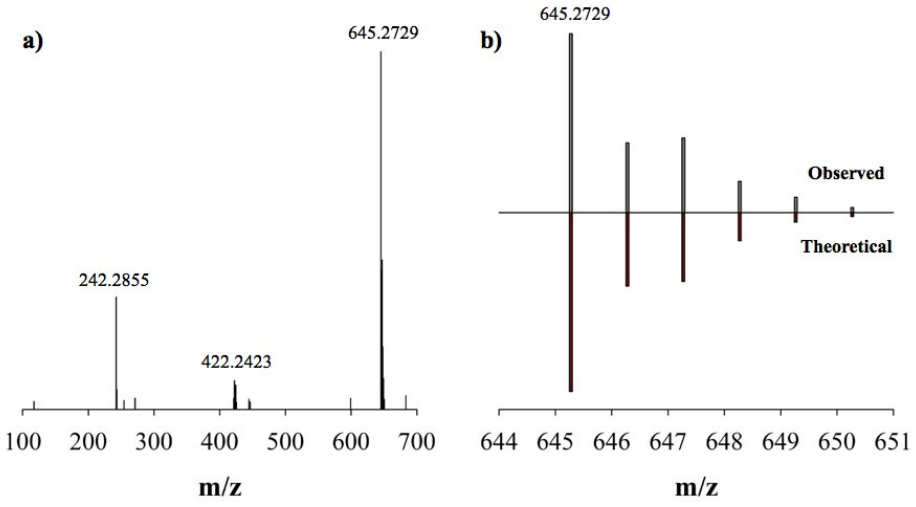

Figure S13. a) Mass spectrometry of **1**. b) Isotopic pattern distribution of m/z = 645 peak for **1**.

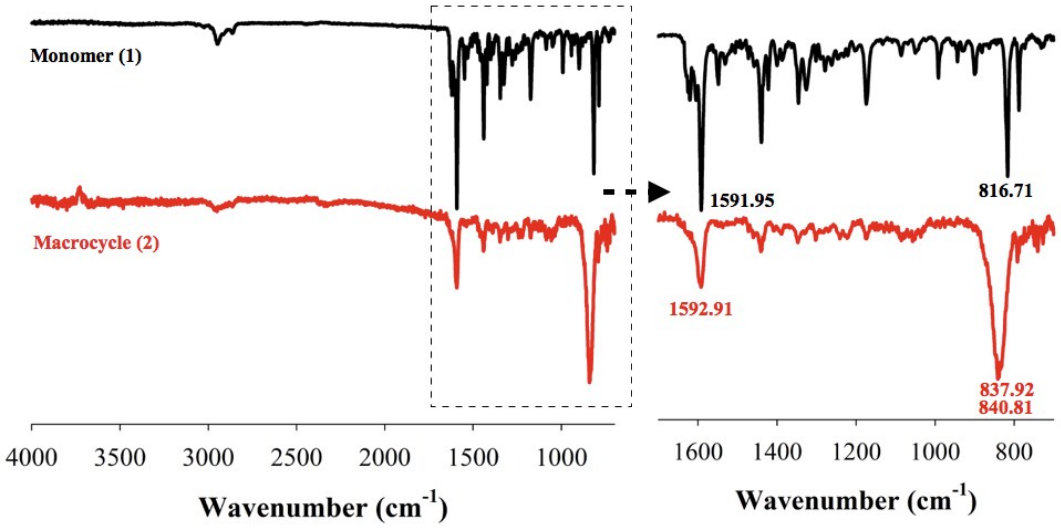

Figure S14. Infrared spectra of **1** and **2**.

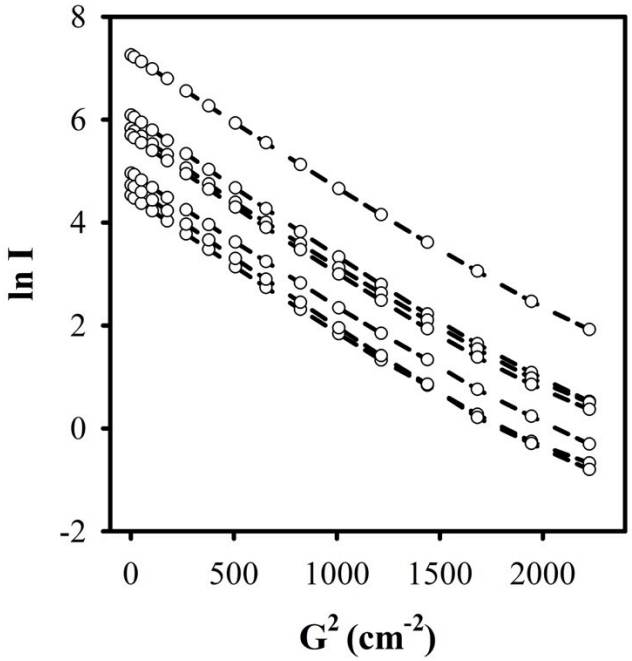

Figure S15. Diffusion profile of **2**. Plot of the peak decay (natural log of the intensity of each peak, ln I) as a function of gradient strength (G^2) of ^{1}H DOSY NMR of **2** in CD_3NO_2. Linear correlation of each peak supports the presence of a unique supramolecular species in the solution with an average diffusion rate (*D*) of 2.45×10^{-10} m^2 s^{-1}.

11.0 References

1. M. T. Ma, H. N. Hoang, C. C. Scully, T. G. Appleton and D. P. Fairlie, *J. Am. Chem. Soc.*, 2009, **131**, 4505-4512.
2. W.-S. Kim, K. Y. Lee, E.-H. Ryu, J.-M. Gu, Y. Kim, S. J. Lee and S. Huh, *Eur. J. Inorg. Chem.*, 2013, 4228-4233.
3. K. Senthil Murugan, T. Rajendran, G. Balakrishnan, M. Ganesan, V. K. Sivasubramanian, J. Sankar, A. Ilangovan, P. Ramamurthy and S. Rajagopal, *J. Phys. Chem. A*, 2014, **118**, 4451-4463.
4. G. A. Morris, H. Zhou, C. L. Stern and S. T. Nguyen, *Inorg. Chem.*, 2001, **40**, 3222-3227.
5. N. G. Connelly and W. E. Geiger, *Chem. Rev.*, 1996, **96**, 877-910.
6. Y. Murata, F. Cheng, T. Kitagawa and K. Komatsu, *J. Am. Chem. Soc.*, 2004, **126**, 8874-8875.
7. I. Noviandri, K. N. Brown, D. S. Fleming, P. T. Gulyas, P. A. Lay, A. F. Masters and L. Phillips, *J. Phys. Chem. B*, 1999, **103**, 6713-6722.
8. H. Sun, W. Chen and A. E. Kaifer, *Organometallics*, 2006, **25**, 1828-1830.
9. Y. Cohen, L. Avram and L. Frish, *Angew. Chem. Int. Ed.*, 2005, **44**, 520-554.
10. L. H. Tong, S. Clifford, A. Gomila, S. Duval, L. Guenee and A. F. Williams, *Chem. Commun.*, 2012, **48**, 9891-9893.
11. S. Goeb, S. Bivaud, P. I. Dron, J. Y. Balandier, M. Chas and M. Salle, *Chem. Commun.*, 2012, **48**, 3106-3108.
12. M. J. Frisch, G. W. Trucks, H. B. Schlegel, G. E. Scuseria, M. A. Robb, J. R. Cheeseman, G. Scalmani, V. Barone, G. A. Petersson, H. Nakatsuji, X. Li, M. Caricato, A. V. Marenich, J. Bloino, B. G. Janesko, R. Gomperts, B. Mennucci, H. P. Hratchian, J. V. Ortiz, A. F. Izmaylov, J. L. Sonnenberg, Williams, F. Ding, F. Lipparini, F. Egidi, J. Goings, B. Peng, A. Petrone, T. Henderson, D. Ranasinghe, V. G. Zakrzewski, J. Gao, N. Rega, G. Zheng, W. Liang, M. Hada, M. Ehara, K. Toyota, R. Fukuda, J. Hasegawa, M. Ishida, T. Nakajima, Y. Honda, O. Kitao, H. Nakai, T. Vreven, K. Throssell, J. A. Montgomery Jr., J. E. Peralta, F. Ogliaro, M. J. Bearpark, J. J. Heyd, E. N. Brothers, K. N. Kudin, V. N. Staroverov, T. A. Keith, R. Kobayashi, J. Normand, K. Raghavachari, A. P. Rendell, J. C. Burant, S. S. Iyengar, J. Tomasi, M. Cossi, J. M. Millam, M. Klene, C. Adamo, R. Cammi, J. W. Ochterski, R. L. Martin, K. Morokuma, O. Farkas, J. B. Foresman and D. J. Fox, Gaussian 16 Rev. B.01, 2016.
13. (a) P. J. Stephens, F. J. Devlin, C. F. Chabalowski and M. J. Frisch, *J. Phys. Chem.*, 1994, **98**, 11623-11627; (b) A. D. Becke, *J. Chem. Phys.*, 1993, **98**, 5648-5652.
14. P. J. Hay and W. R. Wadt, *J. Chem. Phys.*, 1985, **82**, 270-283.
15. (a) J. Tomasi, B. Mennucci and E. Cances, *J. Mol. Struct.*, 1999, **464**, 211-226; (b) V. Barone, M. Cossi and J. Tomasi, *J. Comput. Chem.*, 1998, **19**, 404-417; (c) V. Barone, M. Cossi and J. Tomasi, *J. Chem. Phys.*, 1997, **107**, 3210-3221; (d) S. Miertus, E. Scrocco and J. Tomasi, *Chem. Phys.*, 1981, **55**, 117-129.
16. (a) R. E. Stratmann, G. E. Scuseria and M. J. Frisch, *J. Chem. Phys.*, 1998, **109**, 8218-8224; (b) M. E. Casida, in *In Recent Advances in Density Functional Methods*, ed. D. P. Chong, World Scientific, Singapore, 1995, p. 155.
17. (a) A. Schafer, C. Huber and R. Ahlrichs, *J. Chem. Phys.*, 1994, **100**, 5829-5835; (b) A. Schafer, H. Horn and R. Ahlrichs, *J. Chem. Phys.*, 1992, **97**, 2571-2577.

18. A. K. Rappe, C. J. Casewit, K. S. Colwell, W. A. Goddard and W. M. Skiff, *J. Am. Chem. Soc.*, 1992, **114**, 10024-10035.

12.0 Computational Data

12.1 Optimized Coordinates (Å) for [fragment]$^{\bullet+}$

N	-9.68662325	-0.48835413	-0.15043466
C	-8.97343927	-1.41468404	0.52204476
C	-9.02464643	0.44305068	-0.86710896
C	-7.58732794	-1.43969639	0.49747043
H	-9.53527290	-2.14502026	1.09212622
C	-7.64085449	0.47300517	-0.93975688
H	-9.63088702	1.16851270	-1.39689110
C	-6.87355160	-0.48158913	-0.24630787
H	-7.07775946	-2.19617864	1.08240699
H	-7.17396410	1.22901412	-1.56018099
C	-5.39673734	-0.47386742	-0.29430768
C	-4.68828856	0.70292837	-0.49778206
C	-4.65719988	-1.67375914	-0.11651841
C	-3.28428524	0.69465534	-0.52628189
H	-5.20183920	1.65356315	-0.59962917
C	-3.27471826	-1.75430731	-0.13290842
H	-5.21801871	-2.58870889	0.01778249
C	-2.61159987	1.94207758	-0.70918036
C	-2.54623980	-0.52553532	-0.35571532
C	-2.55095522	-3.09565172	0.07785002
N	-1.32481605	2.11408450	-0.71727677
H	-3.24568438	2.81431203	-0.85145664
O	-1.24569227	-0.53377607	-0.40105947
C	-1.71049968	-3.43903269	-1.17600906
C	-3.53804315	-4.25899696	0.30502733
C	-1.65161274	-3.00314311	1.33628841
Ni	-0.02954765	0.82095722	-0.50448692
C	-0.72207869	3.45488904	-0.92227098
H	-0.96180155	-2.67431047	-1.38352402
H	-1.19301060	-4.39285871	-1.02250803
H	-2.35670533	-3.54430662	-2.05555397
H	-4.16145267	-4.10758600	1.19391205
H	-4.19333269	-4.42225185	-0.55828680
H	-2.96673108	-5.18013265	0.45934685
H	-0.91168660	-2.20572904	1.25195317
H	-2.25950916	-2.81972775	2.23007270
H	-1.12017674	-3.95072558	1.47952548
O	1.28162897	-0.44051603	-0.65384841
N	1.16426611	2.19350304	-0.20388522
C	0.46652350	3.47926390	0.04611234

C	-1.63486648	4.66955216	-0.74401303
H	-0.32011217	3.45480495	-1.94495454
C	2.57916479	-0.34010741	-0.64226632
C	2.45911672	2.10626627	-0.16465190
C	1.29178739	4.76073810	-0.08429016
H	0.06360131	3.41327085	1.06640698
C	-0.80786951	5.96169432	-0.87922781
H	-2.10922294	4.63247435	0.24549741
H	-2.43036236	4.66589416	-1.49695625
C	3.40337263	-1.49970092	-0.90206200
C	3.22143184	0.91565193	-0.36887234
H	3.02672424	3.01098205	0.04186894
C	0.37598124	5.98597478	0.09516434
H	2.08437059	4.78625208	0.67124678
H	1.77011434	4.79161192	-1.07202207
H	-0.43862274	6.05086482	-1.90972516
H	-1.46058709	6.82314959	-0.70319450
C	4.77561399	-1.33108122	-0.81692029
C	2.78819395	-2.86799482	-1.24474062
C	4.62059560	1.01406357	-0.29898535
H	0.96633742	6.89690277	-0.04947627
H	0.00294695	6.01234638	1.12801605
C	5.41855722	-0.10230157	-0.50781888
H	5.40455350	-2.19813067	-0.96803039
C	1.93979227	-3.36763493	-0.05066243
C	1.91856230	-2.74330587	-2.52085218
C	3.86556753	-3.93507871	-1.52800297
H	5.06096204	1.98674575	-0.10555964
C	6.89039722	-0.01921338	-0.40978187
H	1.13510823	-2.67290899	0.19039008
H	1.49286245	-4.33816322	-0.29452123
H	2.56682118	-3.49940059	0.83914592
H	1.10603602	-2.02643362	-2.39365019
H	2.52971746	-2.42836181	-3.37489090
H	1.48088663	-3.71839125	-2.76228300
H	4.50799466	-3.66281709	-2.37372339
H	4.49951129	-4.12767475	-0.65491307
H	3.36926795	-4.87707094	-1.78342268
C	7.51721513	0.92778044	0.42140094
C	7.73815283	-0.88158441	-1.12952773
C	8.89929831	0.97753367	0.50530314
H	6.93994102	1.61288424	1.03113345
C	9.11489327	-0.78343585	-0.99133915
H	7.34066784	-1.62102606	-1.81445415
H	9.39460541	1.69926813	1.14349923
N	9.69091303	0.13099324	-0.18411777

H	9.78197888	-1.44407519	-1.53335966
Pd	-11.76416562	-0.47661163	-0.05901230
N	-11.98163148	-1.74056492	-1.71235558
H	-11.33528143	-1.50543118	-2.46739705
N	-13.85841088	-0.51914898	-0.08480013
H	-14.18370884	0.38420640	-0.43749322
C	-14.31503036	-1.62701225	-0.98331280
H	-15.35539003	-1.47376642	-1.28443078
H	-14.25600662	-2.55739394	-0.41316871
C	-13.39784241	-1.66740795	-2.19291840
H	-13.63032866	-2.51926881	-2.83833096
H	-13.49436646	-0.75064337	-2.78040774
H	-11.74596827	-2.69238039	-1.42161268
H	-14.26171808	-0.62250895	0.84755085
Pd	11.75666553	0.22587973	0.02557732
N	13.83985073	0.39420020	0.11451006
H	14.18379017	0.48892037	1.07171731
N	11.98215521	1.53934312	-1.58683029
H	11.66507781	2.46288399	-1.28305599
C	13.42567645	1.58243182	-1.98111284
H	13.63496706	2.47251689	-2.58131960
H	13.62382444	0.69872044	-2.59305729
C	14.26500686	1.56498487	-0.71518012
H	15.33197579	1.50534107	-0.94754006
H	14.08940654	2.46531572	-0.12127589
H	14.24313412	-0.47129479	-0.25135558
H	11.39724575	1.28236876	-2.38336500
C	11.56263635	-0.57383652	2.90232451
C	11.75379512	-2.39592724	1.46135874
C	11.52092506	-1.40999681	4.01234665
H	11.50521040	0.50364148	3.00158340
C	11.71711631	-3.28884128	2.52606995
H	11.84344171	-2.73580778	0.43660605
C	11.59918127	-2.79011979	3.82373415
H	11.43042998	-0.97735316	5.00224434
H	11.78154004	-4.35339619	2.33136525
H	11.56972944	-3.46472669	4.67318175
C	-11.67994309	2.12979510	1.39676222
C	-11.61437475	0.29438831	2.83127853
C	-11.61070411	3.01506007	2.46613386
H	-11.73887920	2.47826010	0.37226808
C	-11.54354749	1.12205545	3.94614136
H	-11.62493458	-0.78526015	2.92323730
C	-11.54106930	2.50510135	3.76304142
H	-11.61379821	4.08225231	2.27540024
H	-11.49301773	0.68114432	4.93519124

H	-11.48776279	3.17348339	4.61626254
N	11.67749083	-1.06306357	1.65109661
N	-11.68311037	0.79356836	1.58094366

12.2 TD-DFT Excitation Energies and Oscillator Strength for [fragment]$^{\bullet+}$

Excited State 1: 2.019-A 0.6495 eV 1908.81 nm f=0.2318 <S2>=0.769**
249B -> 263B -0.15379
250B -> 263B -0.21368
260B -> 263B 0.24549
262B -> 263B 0.92332
This state for optimization and/or second-order correction.
Total Energy, E(TD-HF/TD-DFT) = -4482.63623683
Copying the excited state density for this state as the 1-particle RhoCI density.

Excited State 2: 2.020-A 0.8958 eV 1384.11 nm f=0.0000 <S**2>=0.770
247B -> 263B -0.11541
253B -> 263B 0.52405
256B -> 263B 0.74580
257B -> 263B -0.33777

Excited State 3: 3.165-A 1.0936 eV 1133.70 nm f=0.0516 <S**2>=2.254
251A -> 264A 0.11306
254A -> 264A 0.49485
257A -> 264A 0.24416
249B -> 263B -0.19376
250B -> 263B -0.20469
253B -> 266B -0.40988
253B -> 267B 0.13257
256B -> 266B -0.39266
256B -> 267B 0.13546
257B -> 266B 0.24886
260B -> 263B 0.32895
262B -> 263B -0.22081
254A <- 264A 0.13487
253B <- 266B -0.12281
256B <- 266B -0.10645

Excited State 4: 2.456-A 1.1966 eV 1036.15 nm f=0.1247 <S2>=1.258**
254A -> 264A -0.39276
257A -> 264A -0.14340
249B -> 263B -0.30552
250B -> 263B -0.33782
253B -> 266B 0.14966
256B -> 266B 0.16980
260B -> 263B 0.61477
261B -> 263B -0.16647

262B -> 263B -0.29005

Excited State 5: 2.050-A 1.2485 eV 993.05 nm f=0.0189 <S**2>=0.801
253B -> 263B -0.13416
256B -> 263B 0.13428
257B -> 263B 0.31528
260B -> 263B 0.14446
261B -> 263B 0.87038

Excited State 6: 3.417-A 1.3642 eV 908.84 nm f=0.0008 <S**2>=2.669
237A -> 264A -0.10936
246A -> 264A 0.54671
258A -> 264A 0.27756
262A -> 264A 0.18878
249B -> 266B -0.34089
249B -> 267B 0.11716
250B -> 266B -0.41894
250B -> 267B 0.14192
256B -> 263B -0.10261
260B -> 266B 0.32098
261B -> 263B 0.16145
262B -> 266B 0.19243
246A <- 264A 0.12220

Excited State 7: 2.899-A 1.5141 eV 818.85 nm f=0.0001 <S**2>=1.851
224A -> 264A -0.15968
226A -> 264A 0.13444
231A -> 264A 0.13076
234A -> 264A 0.24059
236A -> 264A 0.10529
238A -> 264A -0.11644
240A -> 264A 0.11203
245A -> 264A -0.16599
251A -> 264A 0.18755
254A -> 264A -0.12737
257A -> 264A 0.15796
259A -> 264A 0.19053
263A -> 264A 0.46919
241B -> 266B -0.16090
247B -> 266B 0.14323
253B -> 266B -0.11955
257B -> 266B -0.28800
261B -> 266B -0.45573
261B -> 267B 0.15034

Excited State 8: 2.086-A 1.5338 eV 808.35 nm f=0.0060 <S**2>=0.838

246A -> 264A 0.17813
233B -> 263B -0.22094
253B -> 263B -0.38631
256B -> 263B 0.55821
257B -> 263B 0.52350
261B -> 263B -0.34281

Excited State 9: 2.029-A 1.9318 eV 641.81 nm f=0.0013 <S**2>=0.779
233B -> 263B 0.11673
241B -> 263B 0.17848
247B -> 263B -0.23257
253B -> 263B 0.59031
256B -> 263B -0.15042
257B -> 263B 0.67011
261B -> 263B -0.15344

Excited State 10: 2.032-A 1.9692 eV 629.62 nm f=0.0017 <S**2>=0.782
254A -> 264A 0.10653
249B -> 263B 0.42389
250B -> 263B 0.59139
260B -> 263B 0.63020